Hindawi
Complexity
Volume 2020, Article ID 2706091, 15 pages
https://doi.org/10.1155/2020/2706091

Research Article

Damage Characteristics and Constitutive Model of Deep Rock under Frequent Impact Disturbances in the Process of Unloading High Static Stress

Chun Wang,[1,2,3,4] **Shuai-fei Zhan**,[1] **Mei-zhi Xie**,[2,5] **Cheng Wang**,[1,3] **Lu-ping Cheng**,[1,3,6] **and Zu-qiang Xiong**[1]

[1]*School of Energy Science and Engineering, Henan Polytechnic University, Jiaozuo, Henan 454000, China*
[2]*Guangxi Key Laboratory of Disaster Prevention and Engineering Safety, Guangxi University, Nanning, Guangxi 530029, China*
[3]*State and Local Joint Engineering Laboratory for Gas Drainage & Ground Control of Deep Mines, Henan Polytechnic University, Jiaozuo, Henan 454000, China*
[4]*The Collaborative Innovation Center of Coal Safety Production of Henan, Jiaozuo, Henan 454000, China*
[5]*College of Civil Engineering and Architecture, Guangxi University, Nanning, Guangxi 530029, China*
[6]*School of Resources and Safety Engineering, Central South University, Changsha, Hunan 410083, China*

Correspondence should be addressed to Mei-zhi Xie; xmzgxdx@163.com, Cheng Wang; 23754987@qq.com, and Lu-ping Cheng; 775174918@qq.com

Received 18 December 2019; Revised 14 March 2020; Accepted 27 March 2020; Published 30 May 2020

Academic Editor: Saleh Mobayen

During the mining of deep mineral resources, the rock is in the complex mechanical environment of high crustal stress and blasting excavation unloading, and the improved SHPB test system is used to carry out frequent impact disturbance test of deep rock in the process of unloading high static stress. Firstly, the general characteristics of dynamic stress-strain curve envelope of the whole process trend can be divided into four stages: the stable development stage of micro cracks, the non-stable development stage of micro cracks, the fatigue damage stage, and the fatigue failure stage. Then, the damage variables of the rock are defined by continuous factors, strain equivalence principle and statistical damage theory, which are based on the whole deformation characteristics of rock during the test. And the derived damage variable equation of rock in the damage process is proved to be reasonable, and the damage constitutive model of rock under frequent disturbances in the process of unloading high static stress is established by the combined model method. Finally, the rationality of constitutive equation is verified by test data, which shows that the dynamic stress-strain curve envelope is in good consistency with the theoretical curve of constitutive equation.

1. Introduction

With the rapid development of human economy, various resources are consumed increasingly. While the shallow resources tend to run out, the exploitation of deep resources is urgently needed, especially the deep mineral resources. However, the mining of deep mineral resources is inevitable to make deep rock mass in the complex mechanical environment of high static stress and frequent dynamic disturbances [1]. Furthermore, the static mechanical theory is inadequate to explain some complex deformation characteristics and failure phenomenon of deep rock, so it is urgent to explore suitable theory and method for explaining the mechanical characteristics.

In order to study the mechanical characteristics of deep rock, scholars in the field of rock mechanics have carried out a large number of experiments, involving the damage characteristics and constitutive models of deep rocks under static and dynamic loads. The research on test equipment and data monitoring technology is also paid much attention. The continuous improvement of equipment and data monitoring technology provide a basic guarantee for the

study of the mechanical characteristics of deep rocks. For example, Mobayen and Tchier [2–4] have come up with novel robust adaptive second-order sliding mode tracking control technique and sliding mode disturbance observer control technique, and a nonsingular fast terminal sliding-mode stabilizer was developed. All these laid a foundation for the improvement of dynamic load test technology.

The research on damage characteristics of deep rock mainly refers to damage variables, damage process, damage mechanics and so on. From the perspective of energy, the laws of energy dissipation in the process of rock deformation and failure are studied by some scholars, which can reflect the damage process effectively [5–7]. Therefore, the method to describe damage variables of rock is defined according to the law of energy dissipation, and the theoretical formula of damage variables is deduced to estimate the damage degree of rock under specific mechanical conditions [8–10]. Based on the mechanical parameters of rocks, damage variables are also defined by elastic modulus method, maximum strain method and residual strength method, and the corresponding formulas of damage variables are inferred, but none of them can reflect the initial damage degree of rocks under frequent disturbances high static stress absolutely [11–14]. As to damage mechanism, partial scholars have also discussed the influence of temperature, stress environment, and humidity on rock failure characteristics. It is found that high temperature induces germination and expansion of micro-cracks within rock and weakens the strength of rocks [15, 16]. When the stress environment is different, the direction and form of crack germination or expansion in rock internal are different, so the ultimate failure modes are different too [17, 18]. Moreover, rock with higher water content is more vulnerable to damage [19, 20].

As regards with the constitutive model of deep rock, it involves the research of influencing factors, model establishment, equation deduction and so on. Because rock is the product of geological process, its characteristics affected mechanical properties are discontinuous, anisotropic inhomogeneous etc. For example, the rock strength under impact load is much greater than that under static stress [21–23], and the rock changes from brittleness to toughness under high confining pressure [24–27]. Therefore, it can be see that there are many complex factors which affect the rock constitutive model, and a large number of studies have been carried out by scholars. Considering the interaction of temperature, residual strength and mechanical conditions, a thermo-mechanical coupled damage model [28, 29] and thermal damage model [30, 31] are established, providing theoretical reference for the excavation and drilling of deep rock mass engineering. Due to the influence of water content and the pH of water on rock mechanical properties, it is found that the degree of chemical damage caused by water reflects the internal damage of rock to some extent, so a damage constitutive model of fractured rock mass under chemical water-rock environment is established [32, 33]. Scholars have also discussed the constitutive model of rock under high stress and dynamic impact disturbances, such as the non-linear damage creep constitutive model of high stress soft rock, established by the non-linear damage creep characteristics [34, 35]. Rock with high stress has the characteristics of transition from brittleness to ductility, and the damage constitutive model under high stress is established [36]. Considering the dual action of temperature and dynamic coupling, the rock mechanical behavior is analyzed to study rock constitutive model under this condition [37, 38].

In summary, a lot of studies have been carried out on rock damage characteristics and constitutive models in different mechanical environments, and the results obtained are used to guide the corresponding engineering practice, for example, Liu and Dai [39] proposes a damage constitutive model describing the deformation and strength characteristics of fractured rock mass under cyclic uniaxial compression. Liu et al. [40] establish a damage constitutive model describing rock mechanical behavior under cyclic loading, based on the law of energy dissipation. The research on damage characteristics and constitutive model of deep rocks under the action of frequent impact loads is insufficient, especially the study on the damage characteristics and constitutive model of deep rock under frequent impact disturbances in the process of unloading high static stress. During the deep rock engineering construction, the ore body and surrounding rock are under the condition of high in-situ stress, especially the mining engineering. The mechanical properties of deep rock will change under the influence of frequent impact disturbance caused by blasting excavation. At the same time, the equilibrium state of the original rock stress is broken during the blasting excavation operation. Therefore, during the formation of the new stress equilibrium state, the ore and surrounding rock are in the process of unloading. Based on the above mentioned analysis, the environment of the engineering rock mass can be summarized as follows: the deep rocks are subjected to frequent impact disturbance in the process of high-stress unloading. Therefore, an experimental study on the damage characteristics and constitutive model of deep rock based on the actual engineering environment which was carried out can provide a theoretical reference for the rock breaking and support in deep rock mass engineering construction.

To solve these problems, experimental research is carried out on some new ideas. Such as, the high static load applied in the axial direction of the rock sample is used to simulate the high in-situ stress of deep rock, the excavation unloading process of rock mass engineering is simulated by unloading high static load at different rates, and the impact loads frequently applied up the rock sample axis is used to simulate the impact disturbance caused by multiple blasting. At the same time, the growth model of biological population introduced to analyze the microcrack propagation in rock is the first time. In this way, the damage characteristics of rock can be quantitatively analyzed, and the dynamic constitutive relationship of deep rock can be established under the corresponding conditions. Finally, the purpose of guiding deep rock engineering construction is realized.

2. High Static Load Unloading Frequent Impact Disturbance Test

2.1. Test Specimen and Equipment

2.1.1. Test Specimen. The test core was taken from the surrounding rock near mining roadway in the depth of 900m underground of Dongguashan Copper Mine, and it was skarn with dense structure and good homogeneous by analysis. To ensure that the non-parallelism and non-perpendicularity of specimens were less than 0.02 mm, the two ends of them were carefully polished. Specimens were processed into two kinds of sizes (50 mm × 100 mm, 50 mm × 50 mm), with a high diameter ratio of 2 : 1, which were used to measure the uniaxial compressive strength. In addition, the specimens with a high diameter ratio of 1 : 1 were used to study the frequent disturbances test of high static stress unloaded.

2.1.2. Test Equipment. Both the uniaxial compressive test and high static stress unloaded test were completed in Central South University, and the former was studied by Instron1346 type electro-hydraulic servo testing machine, while the latter relied on the improved SHPB test system (Structure diagram as shown in Figure 1 [41]) for research. As shown in Figure 1, the improved SHPB test system is capable of axial loading and unloading. Manual hydraulic pump is used for loading, and the loading time can be recorded with a stopwatch to control the loading rate. The hydraulic valve needs to be opened slowly when the pressure is unloaded, moreover, the unloaded value and time are recorded to control the unloaded speed.

2.2. Test Scheme.

For simulating high static stress state, the basic principle is that pre-added axial pressure is set as close as possible to the uniaxial compressive strength, and the axial pressure is unloaded at different rates to simulate the process of rock excavation. In order to ensure that the specimens can withstand multiple cyclic impacts, as soon as the axial pressure is reduced to 50% of pre-added high axial pressure, the impact load of 0.5 MPa is applied to specimens for simulating small disturbance. Before the impact load, the rock sample is first subjected to axial static load. The loading rate first was 0.5 MPa/s, and then changed to 0.1 MPa/s. In order to prevent the rock sample from being damaged because the loading rate is too fast, the loading rate is adjusted to 0.1 MPa/s when the later axial pressure of 5 MPa is applied. At the same time, in order to ensure the same impact load rate in the test, the heterotype impact hammer were placed at the same position in launch cavity before each impact. Then when the impact pressure is fixed, the impact load can be kept constant, which was applied to the impact end of the incident bar. Test scheme is shown in Tables 1 and 2, and the average uniaxial compressive stress of skarn is 126.63 MPa according to the data of Table 1.

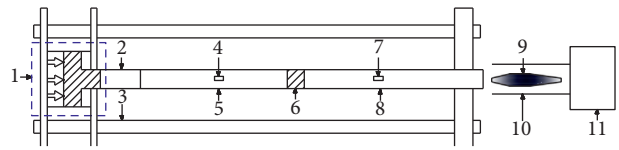

Figure 1: Structure diagram of the test load: (1) Pressure loading unit; (2) Buffer bar; (3) Support; (4) Strain gauge A2; (5) Transmission bar; (6) Rock specimen; (7) Strain gauge A1; (8) Incident bar; (9) Heterotype impact hammer; (10) Launch cavity; (11) Gas gun.

2.3. Test Results. According to the differences of preadded axial pressures and unloading rate, the test was divided into 16 groups. Each specimen was subjected to multiple impact disturbances, and the corresponding dynamic stress-strain curves can be obtained after each impact disturbances. To study the overall deformation characteristics of specimen, the envelope of the dynamic stress-strain curve of each specimen under multiple impact disturbances was selected for analysis. In the test, a corresponding dynamic stress-strain curve can be drawn based on the test data obtained from each impact. Some feature data can be selected to form a new set of data, such as the peak data and all data before the peak on the stress-strain curve obtained at the first impact, the data corresponding to the residual strength stage after the peak at the last impact, and the peak data on the dynamic stress-strain curve corresponding to the intermediate impacts. The stress-strain curve drawn with the new data combination is the envelope curve of the dynamic stress-strain curve. Figure 2 shows some representative dynamic stress-strain curves, in which the numbers represent the disturbance times. Figure 3 lists the envelopes of dynamic stress-strain curves at the unloading rate of 0.5 MPa/s and the pre-added axial pressure of 85 MPa, respectively. In Figure 3(a), the numbers represent pre-added axial pressure value, and the numbers in Figure 3(b) show unloading rate of axial pressure.

It can be seen from Figure 2 that, the initial stages of dynamic stress-strain curves are approximately linear, the straight-line segment is gradually shortened with the increasing impact disturbance times, and the speed entering nonlinear stage is getting faster. It indicates that the specimen appears to have elastic deformation firstly and then plastic deformation under high static stress unloaded and frequent disturbances, and the elastic properties in specimen are weakened through frequent disturbances. Because the micro cracks in specimen are closed almost under pre-added high axial pressure, there is no compaction stage, and the specimen enters the elastic stage directly. Moreover, the pre-added axial pressure approached the uniaxial compressive strength extremely, which leads to damage in specimen, in the meantime, the damage is gradually aggravated by loading, unloading and frequent disturbances. Therefore, the elastic deformation stage becomes shortened and the plastic deformation stage enlarged gradually on dynamic stress-strain curve. Figure 2 also shows that the trends of envelope of the dynamic stress-strain curves are consistent with that of dynamic stress-strain curve at each impact, which shows

Table 1: Test scheme and results of deep skarn under uniaxial compression.

Number	Height (mm)	Diameter (mm)	Density (g/cm^3)	Longitudinal wave velocity (m/s)	Loading rate (mm/s)	Peak load (kN)	Uniaxial compressive strength (MPa)
XK1	100.02	50.06	3.78	5567	0.03	239.08	121.53
XK2	99.36	49.86	4.26	5898	0.03	384.10	196.82
XK3	99.24	49.56	4.06	5324	0.03	255.80	132.67
XK4	98.96	49.98	3.84	5126	0.03	176.93	90.23
XK5	100.02	50.02	3.72	5297	0.03	252.89	128.76
XK6	99.04	49.94	3.94	5135	0.03	220.17	112.46
XK7	100.08	50.04	3.90	5079	0.03	204.31	103.94

Table 2: Test scheme of high static stress unloaded and frequent disturbances.

Number	Height (mm)	Diameter (mm)	Density (g/cm^3)	Longitudinal wave velocity (m/s)	Pre-axial pressure (MPa)	Axial pressure on impact (MPa)	Unloading rate of axial pressure (MPa/s)	Impact pressure (MPa)
XK1-1	50.34	53.60	3.10	4467	65	32.5	0.5	0.5
XK1-2	50.22	52.98	3.09	4549	75	37.5		
XK1-3	49.85	52.88	3.33	4674	85	42.5		
XK1-4	49.85	53.70	3.39	4496	95	47.5		
XK2-1	49.47	53.08	3.56	4310	65	32.5	1.0	0.5
XK2-2	49.81	52.87	3.22	4625	75	37.5		
XK2-3	50.05	53.72	3.53	4613	85	42.5		
XK2-4	50.07	53.14	3.54	4428	95	47.5		
XK3-1	49.74	53.15	3.19	4563	65	32.5	1.5	0.5
XK3-2	50.07	53.69	3.52	4146	75	37.5		
XK3-3	49.41	53.20	3.30	4567	85	42.5		
XK3-4	49.67	53.34	3.51	4366	95	47.5		
XK4-1	50.30	53.36	2.94	4743	65	32.5	2.0	0.5
XK4-2	50.30	53.24	3.21	4571	75	37.5		
XK4-3	49.71	53.26	2.85	4227	85	42.5		
XK4-4	49.59	53.31	3.53	4252	95	47.5		

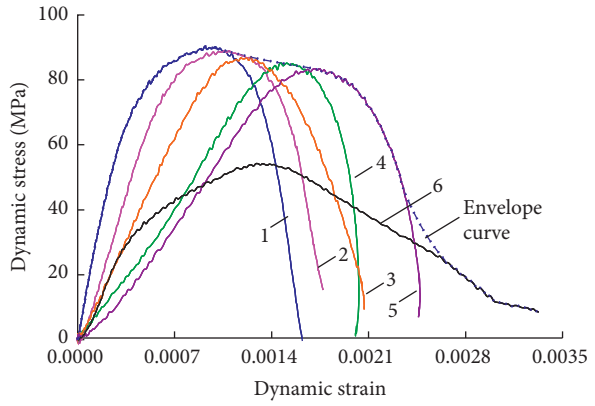

Figure 2: Dynamic stress - strain curve and envelope curve of skarn under the common action of high static stress unloading and impact disturbance (axial load 95 MPa and unloading rate 0.5 MPa/s).

that the whole process trends of specimens under same axial pressure, same unloading rate, and same impact strength can be reflected by variation characteristics of envelope in some conditions.

Figure 3(a) shows that the peak stress decreases corresponding to the envelope with the increase of pre-added axial pressure, when the unloading rate is constant. For example, when the preloaded axial pressures were 65 MPa, 75 MPa, 85 MPa and 95 MPa, the corresponding pressures to the peak stress of the envelope of the dynamic stress-strain curve were 115.08 MPa, 110.58 MPa, 104.25 MPa and 90.38 MPa, respectively. Upon further analysis, the peak stress reduction ratio of the corresponding envelope curve is 3.91%, 5.50% and 12.05%, respectively, when the preloaded axial pressure increased from 65 MPa to 75 MPa, from 75 MPa to 85 MPa and from 85 MPa to 95 MPa. Therefore, the internal damage is aggravated by pre-added high axial pressure, namely, the higher the axial pressure is, the weaker the rock resisted to external disturbance will be. In a word, the number of impact disturbances that the specimens can withstand reduces.

Figure 3(b) shows that the change trends of envelopes remains constant basically when the axial pressure is the same, and it goes through a straight line segment first and then enters a non-linear development stage, indicating that the dynamic change trend of rock is not affected by the unloading rate. When the unloading rate is 0.5 MPa/s, 1.0 MPa/s, 1.5 MPa/s and 2.0 MPa/s, the corresponding dynamic peak stress is 104.25 MPa, 103.85 MPa, 103.38 MPa and 103.15 MPa, respectively. The range between dynamic peak stresses varies from 0.2% to 0.5%, showing a small decreasing trend, and it can be concluded that the allowable dynamic stress decreases with the rising unloading rate.

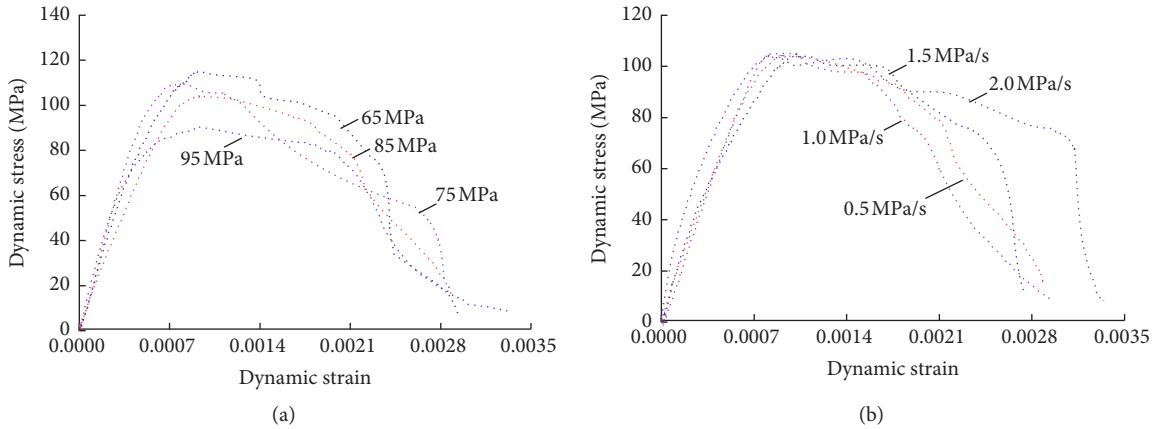

Figure 3: Envelope of typical dynamic stress-strain curve. (a) The axial unloading rate is 0.5 MPa/s. (b) The pre-added axial pressure is 85 MPa.

When the axial pressure is certain, the larger the unloading rate, the shorter the time required for unloading to same axial pressure. The time of specimen affected by the unloading process of high axial pressure is shorter before each impact. At the same time, the time for micro-cracks within specimen to germinate and expand will be shorter, resulting in a smaller internal damage accumulation. In addition, when the specimen is in the process of axial pressure and unloading, it has the effect of delaying the force about external impact. When the unloading rate is higher, the effect of delaying force is more obvious, leading to a decline in effective impact stress and internal fatigue damage on specimens. That is, the higher the unloading rate, the more conducive to stability of rock.

The general characteristics of the envelope of dynamic stress-strain curve can be subdivided into four stages, such as stable development of micro-cracks, unstable development of micro-cracks, fatigue damage, and fatigue failure, as shown in Figure 4.

In the stable development stage of microcracks (OA section), the curve develops in a straight line and the corresponding deformation modulus is the largest, indicating that specimen is in the elastic deformation stage at the beginning. At this stage, the microcracks in specimen are constant or stable, which reflects that the specimen has the maximum impact resistance, and it is more difficult to produce greater deformation.

In the unstable propagation stage of microcracks (section AB), the curve develops in a non-linear way and slows down; meanwhile, the corresponding deformation modulus gradually decreases, indicating that the specimen is in the plastic deformation stage. The internal micro cracks of specimen show instantaneous propagation and transfixion under frequent disturbance, leading to macroscopic failure. However, each dynamic disturbance is small, so a single impact fails to make the micro cracks in specimen through instantly, but makes it in an unstable development.

In the fatigue damage stage (BC segment), this section of the curve shows a downward trend, and the downward trend is relatively slow. At this stage, the rock has a large amount of

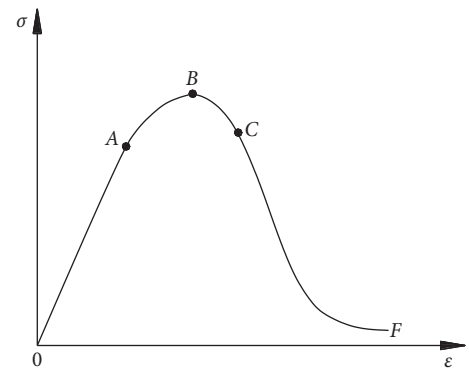

Figure 4: Envelope of typical dynamic stress-strain curve.

compression deformation, but the dynamic stress reduction is relatively small, which shows a certain ductility. Because the elastic energy stored in specimen is relatively large, it is able to counteract part of the frequent disturbance. However, the damage degree in the specimen is still aggravated with the increasing impact numbers, and the elastic energy stored in the specimen decreases gradually, which shows a slow downward trend in the envelope curve.

In the fatigue failure stage (CD segment), the brittleness of the specimen is enhanced. In general, there is no macroscopic failure of the specimen under impact stress, and the leading factor causing macroscopic failure is the pre-added high axial pressure.

3. Analysis of Damage Characteristics

3.1. Damage Variable. In this test, the damage inside the specimen is intensified with each impact, so the reasonable definition of damage variable is helpful to analyze and reflect damage characteristics in the whole test process. Due to the complex internal structure of rock, the rock microelement is assumed to be continuous and random, and the damage variables are defined by continuous factor, strain equivalence principle, or statistical damage theory. Meanwhile, their weighted averages are also used for analysis.

3.1.1. Damage Variable D_1 Based on Continuous Factor and Strain Equivalence Principle. There is a compact structure and good uniformity of test specimen, and it is assumed isotropous in the test. Base on strain equivalence principle, it is considered that the deformation caused by nominal stress acting on the damage material is equal to that caused by effective stress acting on virtual nondestructive material. The schematic diagram of strain equivalence principle for rock microelement is shown in Figure 5.

In summary, the ratio of damage volume to total volume of rock microelement is defined to damage variable D_1, and the formula is as follows:

$$D = 1 - \frac{\widetilde{S}}{S}, \quad 0 \le D \le 1. \tag{1}$$

By combining continuous factor, strain equivalence principle and Hooke's law, the relationship between stress and strain can be obtained from Figure 5:

$$\varepsilon = \frac{\sigma}{\widetilde{E}} = \frac{\widetilde{\sigma}}{E}. \tag{2}$$

Formula (3) is calculated from formulae (1) and (2):

$$D_1 = 1 - \frac{\widetilde{S}}{S} = 1 - \frac{\sigma}{\widetilde{\sigma}} = 1 - \frac{\widetilde{E}}{E}. \tag{3}$$

3.1.2. Damage Variable D_2 Based on Statistical Damage Theory. Assuming that the defects of rock microelement are independent, random, and the distribution of them conforms to Weibull's distribution. Based on statistical damage theory, Tang [42]. Calculated the damage variable of rock, and the formula is as follows:

$$D_2 = 1 - \left[\left(\frac{\varepsilon}{\alpha}\right)^m + 1\right]\exp\left[-\left(\frac{\varepsilon}{\alpha}\right)^m\right], \quad \varepsilon \ge 0. \tag{4}$$

In formula (4), ε, α, and m represents strain of rock damage mass, rock integrity, the and relevant parameters of rock's properties and shapes, respectively.

3.1.3. Damage Variable D under High Static Stress Unloaded and Frequent Disturbances. According to the test results, the damage variable D is rational when the proportion of D_1 and D_2 is 50% respectively, so D is defined as the weighted average among them:

$$D = \frac{D_1 + D_2}{2} = \frac{1}{2}\left\{\left(1 - \frac{\widetilde{E}}{E}\right) + 1 - \left[\left(\frac{\varepsilon}{\alpha}\right)^m + 1\right] \cdot \exp\left[-\left(\frac{\varepsilon}{\alpha}\right)^m\right]\right\}, \quad \varepsilon \ge 0. \tag{5}$$

3.2. Damage Evolution Equation

3.2.1. Equation Analysis of Damage Variable D_1. As the continuous factors and equivalent strain are applied to the definition of damage variable D_1, the following assumptions must be satisfied. Firstly, the rock material is composed of damage and lossless microelements. Secondly, the volume of them is equal, and the lossless microelements are able to irreversibly transform into damage microelements instantaneously. Finally, the damage only occurs along the axial direction but not the laterally, and the lossless microelements obey Hooke's law.

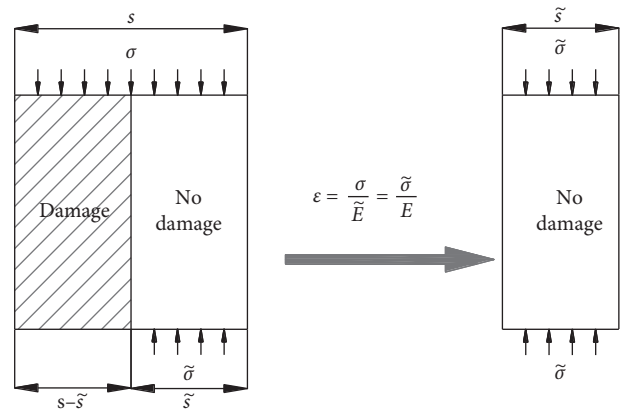

σ: Nominal stress applied to the damaged material
$\widetilde{\sigma}$: Effective stress applied to the no damaged material
$\widetilde{E}$: Elasticity modulus of the damaged material
E: Elasticity modulus of the no damaged material
ε: The strain of a nominal or effective stress on the damaged material or a virtual no damaged material
S: Total area of rock microelement
$\widetilde{s}$: Total area of no damage microelement

Figure 5: The schematic diagram of strain equivalence principle for rock microelement.

Combined with equations (1) and (3), the equation of damage variable can be expressed as:

$$D_1 = \frac{NS_0}{MS_0} = \frac{N}{M}. \tag{6}$$

In formula (6), N is the total number of damaged microelements, M is the sum of the number of nondestructive microelements and damaged microelements, that is, the total number of microelements in the specimen, and S_0 is the volume of a single element.

Assuming that the growth process of biological species group is used to simulate the damage evolution process of rock, the survival environment of species group is considered as rock external load. Moreover, the time in the species group growth model corresponds to the strain of rock under the external load, and the environmental capacity of species group corresponds to the total number of rock microelements, so the growth rate of the number of damaged microelements can be expressed as follows:

$$\frac{\mathrm{d}N}{\mathrm{d}\varepsilon} = rN\left(1 - \frac{N}{M}\right). \tag{7}$$

In formula (7), γ and ε is natural growth rate and the relevant strain of rock, respectively.

Then, formula (7) is solved by the separation of variables in differential equation, and expression (8) is obtained:

$$N = \frac{M}{1 + Ce^{-r\varepsilon}}, \quad C = \frac{M - N_0}{N_0}. \tag{8}$$

In formula (8), N_0 is the initial quantity of rock damage microelements.

The differential formula (9) of damage variable D_1 is deduced by formula (6) and formula (7):

$$\frac{\mathrm{d}D_1}{\mathrm{d}\varepsilon} = \frac{1}{M}\frac{\mathrm{d}N}{\mathrm{d}\varepsilon} = r\frac{N}{M}\left(1 - \frac{N}{M}\right). \tag{9}$$

Substitute formula (8) into formula (7), and formula (10) of damage variable is solved out through the method of separating variables:

$$D_1 = \frac{1}{1 + e^{\beta - r\varepsilon}}, \quad \left[\beta = \ln\left(\frac{M}{N_0} - 1\right)\right]. \tag{10}$$

In formula (10), β represents the initial damage degree of rock material.

3.2.2. Equation Analysis of Damage Variable D_2. According to the statistical damage theory, the distribution of microelement defects in rocks is independent and random, and it satisfies Possion distribution. Therefore, the probability of defects occurrence can be expressed by Possion law within the interval of length l, and the expression of probability function is shown in formula (11) as follows:

$$P\left(\frac{k}{l}\right) = \frac{(\lambda l)^k}{k!}e^{-\lambda l}. \tag{11}$$

In formula (11), λ is the mathematical expectation of microelement defects per unit length, k is the number of microelement defects, and $P(k/l)$ is the probability function of k defects appearing in the interval with length l.

Suppose that the probability of a cell body defect on the length of Δl is $P_1(\Delta l)$, and the probability of no element body defect on the length of l is $P(l)$. Formulae (12) and (13) can be inferred as follows:

$$P_1(\Delta l) = \lambda \Delta l \cdot e^{-\lambda \Delta l}, \tag{12}$$

$$P(l + \Delta l) = P(l) - P(l)P(\Delta l). \tag{13}$$

Formula (14) can be deduced from formulae (12) and (13):

$$\frac{P(l + \Delta l) - P(l)}{\Delta l} = -\lambda P(l) \cdot e^{-\lambda \Delta l}. \tag{14}$$

When $l = 0$, $P(l) = 1$, and the value of Δl tends to zero, so the limit of both sides in formula (14) can be obtained:

$$P(l) = e^{-\lambda l}. \tag{15}$$

Therefore, the probability function $\phi(l)$ for the defect of no less than one microelement in the interval of length l can be derived:

$$\phi(l) = 1 - P(l). \tag{16}$$

The probability density function $\phi(l)$ of microelement can be deduced from formula (16):

$$\varphi(l) = \frac{\mathrm{d}\phi}{\mathrm{d}l} = \lambda e^{-\lambda l}. \tag{17}$$

Assuming that the damage microelement in the specimen loses its bearing capacity and rock strain is infinite when damaged, the expression of damage variable D_2 are represented as follows:

$$D_2 = \frac{\int_0^{\varepsilon} l\varphi(l)\mathrm{d}l}{\int_0^{\infty} l\varphi(l)\mathrm{d}l} = 1 - (\lambda\varepsilon + 1)e^{-\lambda\varepsilon}. \tag{18}$$

While considering the defects of line, plane and body, the completeness was considered as $\alpha = 1/\lambda$ [43]. Therefore, formula (18) can be rewritten as formula (19).

$$D_2 = 1 - \left[\left(\frac{\varepsilon}{\alpha}\right)^m + 1\right]\exp\left[-\left(\frac{\varepsilon}{\alpha}\right)^m\right]. \tag{19}$$

In formula (19), ε is the strain of rock damage mass, and m represents the parameters related to materials and shapes of rock.

3.2.3. Definition of Damage Variable D. Based on the above mentioned equation analysis, the damage variable D of rock under high static stress unloaded and frequent disturbances can be defined as formula (20):

$$D = \frac{1}{2}\left\{1 + \frac{1}{1 + e^{\beta - r\varepsilon}} - \left[\left(\frac{\varepsilon}{\alpha}\right)^m + 1\right]\exp\left[-\left(\frac{\varepsilon}{\alpha}\right)^m\right]\right\}, \quad \left[\beta = \ln\left(\frac{M}{N_0} - 1\right), \varepsilon \geq 0\right]. \tag{20}$$

3.2.4. Determination of Damage Evolution Equation Parameters. If the damage variable D is to be analyzed and calculated, the parameters of β, r, m and α must be determined firstly. To determine the values of β and r, the equation of D_1 needs to be analyzed, while the parameters of m and α can be determined by analyzing the equation of D_2.

(1) Determination of Parameters β and r. Firstly, the value of damage variable D_1 corresponding to each strain of the envelope is calculated by formula (3), then E (the elastic modulus of non-destructive materials) and $\widetilde{E}$ (the elastic modulus of damaged materials) in formula (3) are calculated by Figure 6.

Formula (10) is deduced, and formula (21) is ordered:

$$Y = \ln\left(\frac{1}{D_1} - 1\right) = \beta - r\varepsilon. \tag{21}$$

Calculate the Y value corresponding to each strain in the dynamic stress-strain envelope and then analyze the fitting linear formula (Y-ε linear formula). Finally, by fitting the linear formula (21) with the logistic model, and values of β and r are able to be determined.

(2) Determination of Parameters m and α. Statistical damage theory holds that α (rock integrity) is a function of ε [42], and α is inversely proportional to ε under high static stress unloaded and frequent disturbances as follows:

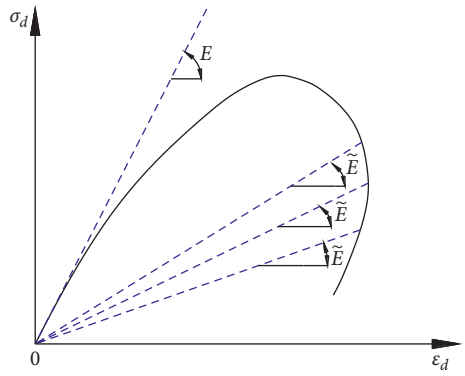

Figure 6: The schematic diagram of E and $\widetilde{E}$ with the determining method.

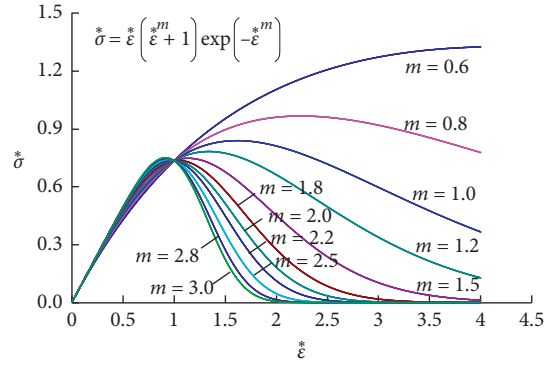

Figure 7: The schematic diagram of dynamic stress-strain curves with one-dimensional dimensionless.

$$\alpha = \frac{C}{\varepsilon}, \quad (C \text{ is a proportionality constant}). \tag{22}$$

Assuming that the equation $\varepsilon/C = 1/\alpha_1$ holds, where α_1 is a parameter related to rock properties and shapes, and substitute it into formula (22), it is found that the values of α and α_1 is equal. Thus, formula (19) can be rewritten to formula (23) as follows:

$$D_2 = 1 - \left[\left(\frac{\varepsilon}{\alpha_1}\right)^m + 1\right]\exp\left[-\left(\frac{\varepsilon}{\alpha_1}\right)^m\right]. \tag{23}$$

It is supposed that the damaged microelement loses its bearing capacity and the non-damaged microelement meets Hooke's law, therefore, the relationship between rock stress and strain under high static stress unloaded and frequent disturbances is shown in formula (24) as follows:

$$\sigma = E\varepsilon(1 - D_2). \tag{24}$$

Substitute formula (23) into formula (24), and formula (25) is given as follows:

$$\sigma = E\varepsilon\left[\left(\frac{\varepsilon}{\alpha_1}\right)^m + 1\right]\exp\left[-\left(\frac{\varepsilon}{\alpha_1}\right)^m\right]. \tag{25}$$

Furthermore, if $\overset{*}{\sigma} = (\sigma/E\alpha_1)$ and $\overset{*}{\varepsilon} = (\varepsilon/\alpha_1)$ are founded, formula (25) can be transformed into dimensionless form, such as formula (26):

$$\overset{*}{\sigma} = \overset{*}{\varepsilon}\left(\overset{*}{\varepsilon}^{m} + 1\right)\exp\left(-\overset{*}{\varepsilon}^{m}\right). \tag{26}$$

According to formula (26), the dynamic stress-strain theoretical curves of rock with different m values are drawn in Figure 7.

By analyzing the similarity of the curves in Figure 7 and the envelope of the measured dynamic stress-strain curves, the value of m can be estimated. After the values of m is determined, the maximum value of $\overset{*}{\sigma}$ is obtained by formula (26), and the parameter α is calculated by formula (27), which is deduced by Tang [42].

$$\alpha = \alpha_1 = \frac{P}{E\overset{*}{\sigma}_{\max}}. \tag{27}$$

In formula (27), P is the peak stress in the envelope of dynamic stress-strain curves.

3.3. Damage Evolution Law. To verify the definition of damage variable D in formula (5), the values of β, r, m and α are substituted into this formula, so the corresponding dynamic damage variable D is calculated by combining the corresponding strain in the envelope of dynamic stress-strain curves. By comparing the damage degree in specimens and analyzing the characteristics of dynamic variable-strain theory curve, it is conclude that the defined damage variable is reasonable. Figure 8 lists the theoretical relationship of two typical damage variable-strain curves, and Figure 9 shows the damage states of the corresponding two groups of rocks during the impact process.

It can be concluded from Figure 8 that

(1) When the value of dynamic strain is 0, the value of damage variable D is greater than 0, so the defined damage reflect the initial damage degree of rock under high static stress.

(2) There exist four stages of fitted damage variable-strain curve, that is moderate increase, fast increase, slowly increase and tend to be stable. The whole curve presents S-shape, and the value of damage variable D is between 0 and 1. It can effectively correspond to four development stages of rock in the test, which is steady development of micro cracks, rapid propagation of micro cracks, fatigue damage and fatigue failure.

(3) When the unloading rate is constant, the greater the axial pressure is, the faster the value of damage variable D tends to be 1, reflecting that pre-high axial pressure accelerates the process of rock damage and failure.

(4) When the pre-loading axial pressure is constant, the smaller the unloading rate is, the faster the damage variable D tends to be 1, which shows that high unloading rate is beneficial to improving the rock' ability to withstand frequent disturbances.

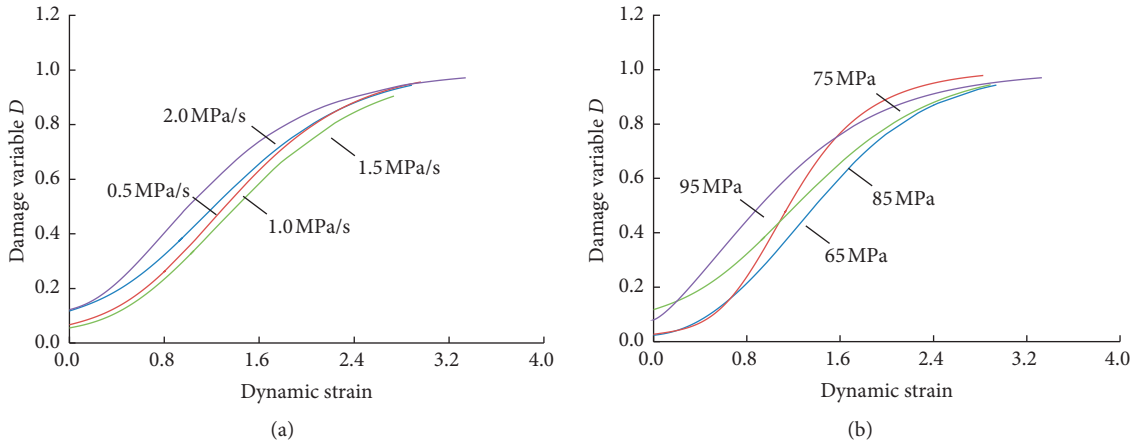

Figure 8: The damage variable-strain curves of rock under high static stress unloaded and frequent disturbances. (a) The axial pressure is 85 MPa. (b) The unloading rate is 0.5 MPa/s.

Figure 9: The damage states of rocks during the impact process. (a) The unloading rate was 0.5 MPa/s and it is the seventh impact. (b) The preloaded axial pressure is 85 MPa and it is the 10th impact.

As shown in Figure 9(a), when the unloading rate and impact times maintain constant, the greater the pre-added axial pressure is, the more serious the rock damage is. When the pre-added axial pressure and impact times keep invariant, the smaller the unloading rate of axial pressure is during the impact process, the more serious the rock damage will be, as shown in Figure 9(b). The above mentioned two phenomena indicate that preadded high axial pressure weakens the ability of rock to resist external impact load, and high unloading rate enhances the ability of rock to withstand frequent disturbances, proving the rationality of defined damage variable.

4. Constitutive Model

4.1. Fundamental Assumption. Based on analysis results of the envelope of rock's dynamic stress-strain curve in this test, the damage evolution law during the impact process is combined to establish the constitutive model under high static stress unloaded and frequent disturbances. However, the establishment of the constitutive model needs to meet certain assumptions, as follows:

(1) The constitutive relationship is not affected by inertia effect at constant train rate [44].

(2) Because the rock element is characterized by elastic-viscous and statistical damage, it is designed as a Maxwell body (composed by an elastic element and a viscous element) which is in parallel with damage body D_{a1} firstly, and then in series with damage body D_{a2}. The mechanical model of rock unit assemblage is shown in Figure 10.

(3) According to the stress state, the constitutive relation of σ and ε is expressed as follows [45]:

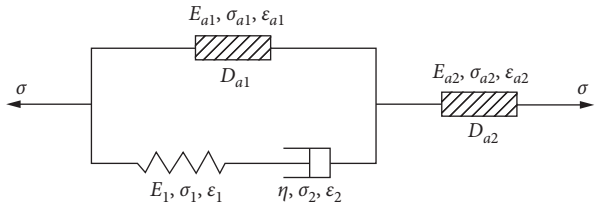

Figure 10: The mechanical model of rock unit assemblage.

$$\sigma = E\varepsilon(1-D)\,(\varepsilon \geq 0). \tag{28}$$

In formula (28), σ and ε are the stress and strain of damage body, respectively.

(4) Because of non-destructive properties, the constitutive relation of viscous element is expressed as follows [46]:

$$\sigma_2 = \eta \frac{d\varepsilon_2}{dt}, \tag{29}$$

In formula (29), σ_2 and ε_2 are the stress and strain of viscous component respectively, η is viscosity coefficient, and t is the time corresponding to strain.

(5) The stress-strain relationship of rock element before damage conforms to the linear differential equation, and it is approximately considered that the principle of strain superposition is still valid [47].

(6) Though the viscoelasticity constitutive equation and the principle of strain equivalence, the influence of damaged rock mass, under high static stress unloaded and frequent disturbances, on constitutive relationship can be predicted [48].

4.2. Establishment of Constitutive Model. In the mechanical model of rock element, the relationship between stress and strain of the viscoelasticity body and damage body is as follows:

$$\left.\begin{aligned} &\sigma = \sigma_{a1} + \sigma_2 = \sigma_{a1} + \sigma_1 = \sigma_{a2}, \\ &\varepsilon = \varepsilon_{a1} + \varepsilon_{a2}, \\ &\varepsilon_{a1} = \varepsilon_1 + \varepsilon_2, \\ &\sigma_1 = \sigma_2. \end{aligned}\right\} \tag{30}$$

In formula (30), σ and ε are the stress, strain of the combined model respectively, σ_{a1} and ε_{a1} are the stress and strain of damage body D_{a1} respectively, σ_{a2} and ε_{a2} are the stress and strain of damage body D_{a2} respectively, σ_1 and ε_1 are the stress and strain of elastic component respectively, σ_2 and ε_2 are the stress and strain of viscous component respectively.

The constitutive equations of Hooke body, viscous body and damaged body are substituted into formula (30), so the constitutive equation of mechanical model of rock assemblage is deduced:

$$\begin{aligned} &\eta\left[E_{a2}(1-D) + E_{a1}(1-D) + E_1\right]\dot{\sigma} + \left[E_1E_{a2}(1-D)\right. \\ &\quad \left. + E_1E_{a1}(1-D)\right]\sigma = \eta\left[E_1E_{a2}(1-D) + E_{a1}E_{a2}(1-D)^2\right]\dot{\varepsilon} \\ &\quad + E_1E_{a1}E_{a2}(1-D)^2\varepsilon. \end{aligned} \tag{31}$$

In formula (31), E_1, E_{a1} and E_{a2} are elasticity modulus of elastic element, damage body D_{a1} and damage body D_{a2} respectively.

The elastic modulus E before damage should be replaced by efficient elastic modulus $E(1-D)$ due to the principle of strain equivalence [49], but the initial damage characteristics are not considered firstly for the better solution of formula (31), that is, the elastic modulus E_{a1} and E_{a2} are adopted to replace $E_{a1}(1-D)$ and $E_{a2}(1-D)$ in formula (31), respectively. Therefore, the constitutive equation of combined model is obtained:

$$\begin{aligned} \eta\left(E_{a2} + E_{a1} + E_1\right)\dot{\sigma} + \left(E_1E_{a2} + E_1E_{a1}\right) \\ \sigma = \eta\left(E_1E_{a2} + E_{a1}E_{a2}\right)\dot{\varepsilon} + E_1E_{a1}E_{a2}\varepsilon. \end{aligned} \tag{32}$$

Because the specimen is subjected to high static pressure, if $t=0$, the initial conditions $\varepsilon(0)=\varepsilon_0$ and $\sigma(0)=F$ are established. Therefore, formula (33) is obtained by Laplace transformation:

$$\begin{aligned} \sigma\left(t+t_0\right) = \frac{E_{a2}\left(E_1+E_{a1}\right)}{E_1+E_{a1}+E_{a2}}\varepsilon\left(t+t_0\right) - \frac{E_1^2E_{a2}^2}{\eta\left(E_1+E_{a1}+E_{a2}\right)^2} \\ \cdot \int_0^t \varepsilon\left(\tau+t_0\right)e^{-\left(E_1E_{a1}+E_1E_{a2}/\eta\left(E_1+E_{a1}+E_{a2}\right)\right)\left(t+t_0-\tau\right)}\mathrm{d}\tau. \end{aligned} \tag{33}$$

In formula (33), t_0 is the loading time of static pressure, and when $t_0=0$, both $\varepsilon(t_0=0)=0$ and $\sigma(t_0=0)=0$ are true.

If $\varepsilon(t+t_0)=\varepsilon_0+\varepsilon_r(t_0)=\varepsilon_0+ct$, where c is constant strain rate and invariable, formula (33) is able to transform into formula (34):

$$\begin{aligned} \sigma\left(t+t_0\right) &= \frac{E_{a2}\left(E_1+E_{a1}\right)}{E_1+E_{a1}+E_{a2}}\left[\varepsilon_0+\varepsilon_r(t)\right] \\ &\quad - \frac{\varepsilon_0E_1E_{a2}^2}{\left(E_{a1}+E_{a2}\right)\left(E_1+E_{a1}+E_{a2}\right)}\left\{e^{At_0} - e^{A\left[\left(\varepsilon_r(t)/c\right)+t_0\right]}\right\} \\ &\quad + \frac{\eta cE_{a2}^2}{\left(E_{a1}+E_{a2}\right)^2}\left\{e^{At_0} - e^{A\left[\left(\varepsilon_r(t)/c\right)+t_0\right]}\right. \\ &\quad \left. - \frac{\left(E_1E_{a1}+E_1E_{a2}\right)\varepsilon_r(t)}{\eta c\left(E_1+E_{a1}+E_{a2}\right)}e^{At_0}\right\}, \end{aligned} \tag{34}$$

where:

$$A = -\frac{E_1\left(E_{a1}+E_{a2}\right)}{\eta\left(E_1+E_{a1}+E_{a2}\right)}. \tag{35}$$

In formula (34), $\varepsilon_r(t)$ is the strain under the interaction of static stress and impact disturbances, ε_0 is the strain produced by static stress F.

Due to the principle of strain equivalence [43], E_{a1} and E_{a2} in formula (34) are replaced by $E_{a1}(1-D)$ and $E_{a2}(1-D)$, and the constitutive equation is calculated as follows:

$$\begin{aligned}\sigma(t+t_0) &= \frac{E_{a2}(1-D)\left[E_1+E_{a1}(1-D)\right]}{E_1+E_{a1}(1-D)+E_{a2}(1-D)}\left[\varepsilon_0+\varepsilon_r(t)\right] \\ &\quad -\frac{\varepsilon_0 E_1 E_{a2}^2(1-D)^2}{(1-D)\left(E_{a1}+E_{a2}\right)\left[E_1+E_{a1}(1-D)+E_{a2}(1-D)\right]} \\ &\quad \cdot\left\{e^{kt_0}-e^{k\left[\left(\varepsilon_r(t)/c\right)+t_0\right]}\right\}+\frac{\eta c E_{a2}^2(1-D)^2}{(1-D)^2\left(E_{a1}+E_{a2}\right)^2} \\ &\quad \cdot\left\{e^{kt_0}-e^{k\left[\left(\varepsilon_r(t)/c\right)+t_0\right]}-\frac{(1-D)\left(E_1E_{a1}+E_1E_{a2}\right)\varepsilon_r(t)}{\eta c\left[E_1+E_{a1}(1-D)+E_{a2}(1-D)\right]}e^{kt_0}\right\},\end{aligned} \tag{36}$$

where:

$$\begin{aligned}D &= D(t+t_0)=1-\left\{\left[\frac{\varepsilon_0+\varepsilon_r(t)}{\alpha}\right]^m+1\right\}\exp\left\{-\left[\frac{\varepsilon_0+\varepsilon_r(t)}{\alpha}\right]^m\right\}, \\ k &= -\frac{E_1(1-D)\left(E_{a1}+E_{a2}\right)}{\eta\left[E_1+E_{a1}(1-D)+E_{a2}(1-D)\right]}.\end{aligned} \tag{37}$$

4.3. Verification of Test Results. For calculating the constitutive equation of rock under high static stress unloaded and frequent disturbances, the values of E_1, E_{a1}, E_{a2}, m, α, η, β, and r need to be determined by analyzing the measured data and carrying out the trial calculation. In the constitutive equation, the strain $\varepsilon_r(t)$, the measured value of static loading time t_0 and the constant strain rate c are test data, where $\varepsilon_r(t)$ is the strain corresponding to the envelope of dynamic stress-strain curve, and t_0 is the average time consumed by pre-added static load before multiple impacts.

According to the test data and the constitutive equation of rock, the following results are obtained: the value of E_1 is similar to deformation modulus of the initial stage of stress-strain curve under first impact in the experimental process, so the former can be substituted by the latter. The value of E_{a1} is able to express by the dynamic deformation modulus $E_{d,}$ and E_d defined as the weighted average of secant modulus, secant modulus of type II and deformation modulus of loading section in the envelope, which is used to reflect the compressive deformation characteristics in the loading stage of rock. Moreover, there is a proportional relationship between E_{a2} and $E_{d,}$ that is $h = E_{a2}/E_d$, where h is dynamic expansion factor. In the test, the action time of impact load is short and the combined dynamic and static resultant force of rock increases rapidly, and the corresponding strain decreases or remains unchanged, which expresses a resilient phenomenon on dynamic stress-strain curve, therefore, the calculated instantaneous dynamic deformation modulus suddenly changes. As a consequence, the ratio h ($h \geq 1$) of transient dynamic deformation modulus E_{a2} and dynamic deformation modulus E_d after mutation is defined as dynamic expansion coefficient, and the value of h can be calculated by the measured data. The four parameters of β, r, m and α are the relative parameters in the damage evolution equation, he viscous coefficient η is deduced according to the fourth basic assumption, and its value range is 500~1000 GPa·s generally.

By analyzing the test data, two groups of typical envelope data of dynamic stress-strain curves are selected for trial calculation, as shown in Table 3.

The parameters in Table 3 are substituted into rock constitutive (36), and the corresponding theoretical dynamic stress-strain curve is fitted and compared with the experimental envelope for analysis, as shown in Figures 11 and 12.

As shown in Figures 11 and 12, when the axial unloading rate or pre-added axial compression remain unchanged, there is a good consistency between theoretical dynamic stress-strain curve and experimental dynamic stress-strain envelope curve. Therefore, the constitutive equation accurately predicts the relationship between dynamic stress and strain of rock in the whole process under high static stress unloaded and frequent disturbances, and indirectly reflects the dynamic deformation characteristics of rock. Moreover, the yield and maximum stress of rock are able to predict effectively by the constitutive equation, as well as the rock deformation corresponding to yield stress, and all these provide theoretical basis for disaster prevention of deep rock excavation engineering.

5. Conclusion

Deep rock mass is in the mechanical environment of high static stress dropped load and frequent impact disturbance during excavation, and the study on damage characteristics and constitutive model of deep rock is carried out, and the main conclusions are as follows:

(1) The envelopes established by dynamic stress-strain curves can reflect the whole variation trend of rock under frequent disturbances in the process of unloading high static stress, as well as the stages of stable development, non-stable expansion, fatigue damage and fatigue failure of rock.

(2) Based on continuous factor, strain equivalence principle and statistical damage theory, the damage variables of rock under frequent disturbances in the process of unloading high static stress are defined, and the methods to determine the parameters of damage variables are deduced. Meanwhile, damage variables defined is proved to be reasonable by experimental data and failure history of rock.

(3) According to the change characteristics of the envelopes of dynamic stress-strain curves, the rock constitutive model under frequent disturbances in the process of unloading high static stress is established with certain assumptions, and the corresponding constitutive equation is deduced. Finally, the experimental curve and theoretical curve of envelope are compared, and it is found that they have good consistency.

5.1. Deficiencies and Suggestions. In the process of studying the damage characteristics and constitutive model of deep rock under frequent impact disturbances in the process of unloading high static stress, it is found that there are some

Table 3: The experimental parameters and theoretical fitting parameters.

Unloading rate ($MPa \cdot s^{-1}$)	F (MPa)	E_1 (GPa)	E_{a1} (GPa)	E_{a2} (GPa)	h (GPa·s)	m	α (10^{-3})	c (10^{-3} s^{-1})	β	r	t_0 (s)	Dynamic expansion coefficient (h)
0.5	65	184.66	135.11	358.04	800	1.21	0.91	20.05	3.05	2216	130	2.65
0.5	75	208.03	165.89	432.96	800	2.08	0.83	23.39	2.87	2122	150	2.61
0.5	85	148.21	124.60	505.88	800	1.48	1.07	20.67	1.18	1515	170	4.06
0.5	95	217.70	150.52	514.77	800	0.82	0.50	19.85	1.67	1865	190	3.42
1	85	144.50	125.13	472.97	800	1.54	1.11	22.54	1.87	1835	170	3.78
1.5	85	151.56	119.56	280.98	800	1.38	1.05	21.67	2.10	1657	170	2.35
2	85	225.99	152.87	502.96	800	1.23	0.68	18.98	1.13	1221	170	3.29

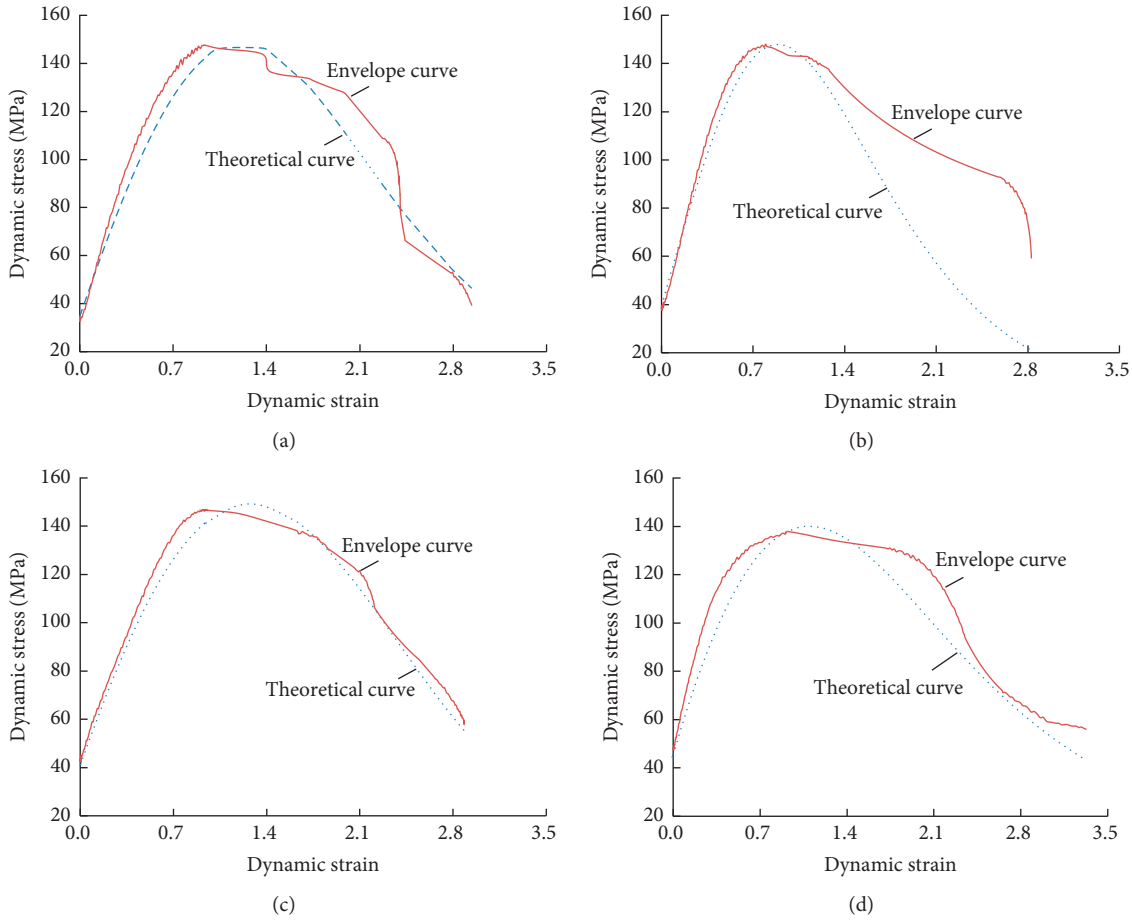

Figure 11: The comparison diagram of theoretical and experimental envelope curves of stress-strain under the axial unloading rate of 0.5 MPa/s. (a) Preload axial pressure 65 MPa. (b) Preload axial pressure 75 MPa. (c) Preload axial pressure 85 MPa. (d) Preload axial pressure 95 MPa.

shortcomings, such as unloading rate control is difficult, the lithology is simple, constitutive equations involve many parameters, and the research results have not been verified by deep rock engineering. Therefore, the following aspects need to be further improved or deepened in the future.

(1) Improve the unloading rate control equipment and reduce the unloading rate control difficulty. At the same time, the damage characteristics and constitutive model of deep rocks need to be further discussed by expanding rock types and increasing the influence of factors such as high temperature.

(2) In order to improve the application of constitutive equation, it is necessary to carry out further research on optimizing the relationship between various parameters and simplifying the expression of constitutive equation.

(3) Based on the specific mechanical characteristics of ore bodies and surrounding rocks in deep rock mass engineering, the quantitative relationship between damage characteristics and constitutive models of deep and deep rocks should be further explored.

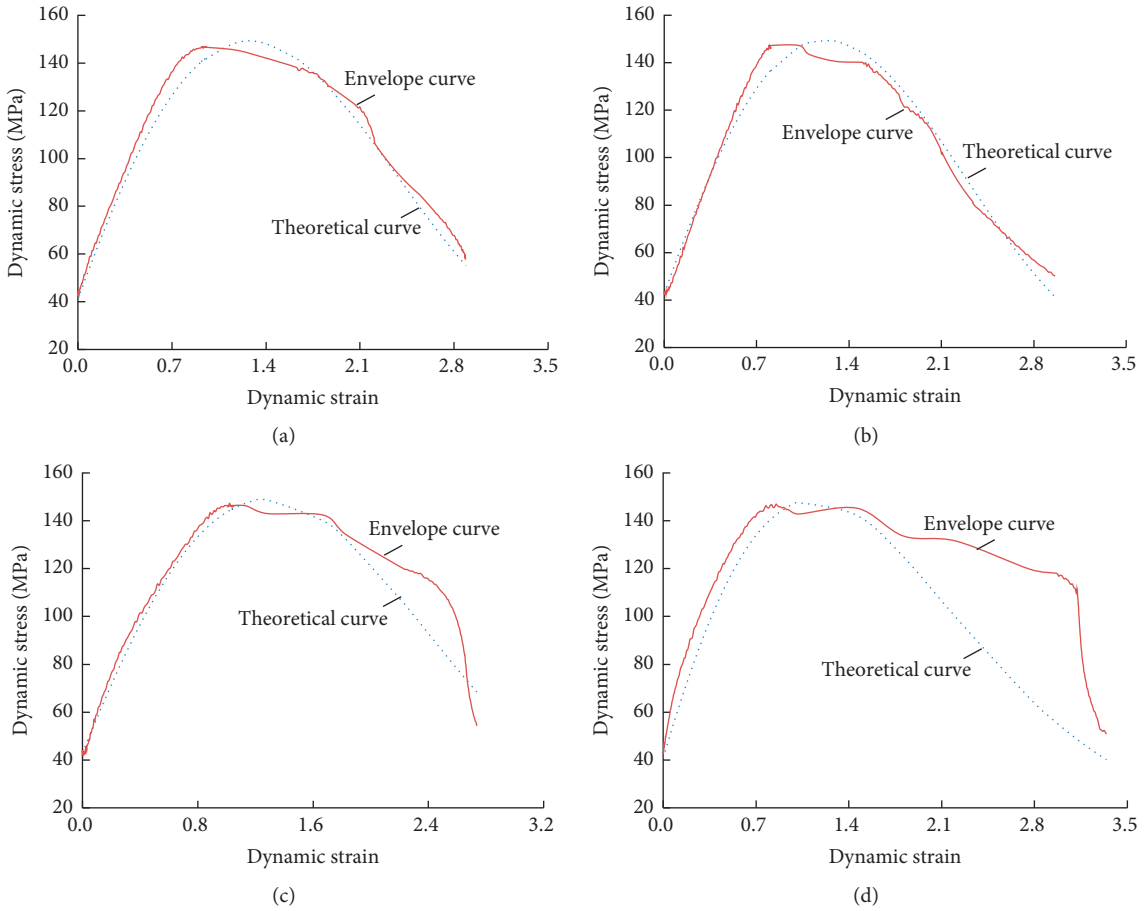

Figure 12: The comparison diagram of theoretical and experimental envelope curves of stress-strain under the pre-added axial compression of 85 MPa (a) axial pressure unloading rate is 0.5 MPa/s. (b) axial pressure unloading rate is 1.0 MPa/s. (c) axial pressure unloading rate is 1.5 MPa/s, and (d) axial pressure unloading rate is 2.0 MPa/s.

Data Availability

All relevant data are within the article and Supporting Information files. The interested researchers can contact via e-mail to wczy115728@163.com.

Conflicts of Interest

The authors declare that they have no conflicts of interest.

Acknowledgments

This work was supported in part by the Systematic Project of Guangxi Key Laboratory of Disaster Prevention and Engineering Safety under Grant 2019ZDK052, Doctoral Foundation of Henan Polytechnic University under Grant 672707, Key Laboratory Open Foundation of Henan Polytechnic University under Grant SJF201802, National Natural Science Foundation of China under Grant 51904093, Key Research and Development and Promotion of Special (Science and Technology) Project of Henan Province under Grant 192102310247, and the Exploration of Youth Innovation Foundation of Henan Polytechnic University under Grant NSFRF180321. The author of the paper is very grateful for the above support.

References

[1] Y. Xu, F. Dai, and H. Du, "Experimental and numerical studies on compression-shear behaviors of brittle rocks subjected to combined static-dynamic loading," *International Journal of Mechanical Sciences*, vol. 175, Article ID 105520, 2020.

[2] S. Mobayen and F. Tchier, "A novel robust adaptive second-order sliding mode tracking control technique for uncertain dynamical systems with matched and unmatched disturbances," *International Journal of Control, Automation and Systems*, vol. 15, no. 3, pp. 1097–1106, 2017.

[3] O. Mofid, S. Mobayen, and M. H. Khooban, "Sliding mode disturbance observer control based on adaptive synchronization in a class of fractional-order chaotic systems," *International Journal of Adaptive Control and Signal Processing*, vol. 33, pp. 462–474, 2018.

[4] S. Mobayen and F. Tchier, "Nonsingular fast terminal sliding-mode stabilizer for a class of uncertain nonlinear systems based on disturbance observer," *Scientia Iranica*, vol. 24, no. 3, pp. 1410–1418, 2017.

[5] T. Li, X. Pei, D. Wang, R. Huang, and H. Tang, "Nonlinear behavior and damage model for fractured rock under cyclic

loading based on energy dissipation principle," *Engineering Fracture Mechanics*, vol. 206, pp. 330–341, 2019.

[6] Y. L. Tan, Q. H. Gu, J. G. Ning, X. S. Liu, Z. C. Jia, and D. M. Huang, "Uniaxial compression behavior of cement mortar and its damage-constitutive model based on energy theory," *Materials*, vol. 12, pp. 1–14, 2019.

[7] F. Gong, J. Yan, X. Li, and S. Luo, "A peak-strength strain energy storage index for rock burst proneness of rock materials," *International Journal of Rock Mechanics and Mining Sciences*, vol. 117, pp. 76–89, 2019.

[8] T. B. Zhou, Y. P. Qin, Q. F. Ma, and J. Liu, "A constitutive model for rock based on energy dissipation and transformation principles," *Arabian Journal of Geosciences*, vol. 12, pp. 1–14, 2019.

[9] T. Wen, H. Tang, J. Ma, and Y. Liu, "Energy analysis of the deformation and failure process of sandstone and damage constitutive model," *KSCE Journal of Civil Engineering*, vol. 23, no. 2, pp. 513–524, 2019.

[10] Y. Lai, M. Liao, and K. Hu, "A constitutive model of frozen saline sandy soil based on energy dissipation theory," *International Journal of Plasticity*, vol. 78, pp. 84–113, 2016.

[11] Y. Gao and X.-T. Feng, "Study on damage evolution of intact and jointed marble subjected to cyclic true triaxial loading," *Engineering Fracture Mechanics*, vol. 215, pp. 224–234, 2019.

[12] K. Zhao, Z. Huang, and B. Yu, "Damage characterization of red sandstones using uniaxial compression experiments," *RSC Advances*, vol. 8, no. 70, pp. 40267–40278, 2018.

[13] H. Zhao, C. J. Shi, M. G. Zhao, and X. B. Li, "Statistical damage constitutive model for rocks considering residual strength," *International Journal of Geomechanics*, vol. 17, pp. 1–9, 2017.

[14] H. Li, H. Liao, G. Xiong, B. Han, and G. Zhao, "A three-dimensional statistical damage constitutive model for geomaterials," *Journal of Mechanical Science and Technology*, vol. 29, no. 1, pp. 71–77, 2015.

[15] M. F. Ahmed, U. Waqas, M. Arshad, and J. D. Rogers, "Effect of heat treatment on dynamic properties of selected rock types taken from the Salt Range in Pakistan," *Arabian Journal of Geosciences*, vol. 11, pp. 1–13, 2018.

[16] Y. Tang, G. Xu, J. Lian, H. Su, and C. Qu, "Effect of temperature and humidity on the adhesion strength and damage mechanism of shotcrete-surrounded rock," *Construction and Building Materials*, vol. 124, pp. 1109–1119, 2016.

[17] X. R. Liu, M. M. Kou, Y. M. Lu, and Y. Q. Liu, "An experimental investigation on the shear mechanism of fatigue damage in rock joints under pre-peak cyclic loading condition," *International Journal of Fatigue*, vol. 106, pp. 175–184, 2018.

[18] L. X. Xie, W. B. Lu, Q. B. Zhang, Q. H. Jiang, G. H. Wang, and J. Zhao, "Damage evolution mechanisms of rock in deep tunnels induced by cut blasting," *Tunnelling and Underground Space Technology*, vol. 58, pp. 257–270, 2016.

[19] X. Sun, H. Xu, L. Zheng, M. He, and W. Gong, "An experimental investigation on acoustic emission characteristics of sandstone rockburst with different moisture contents," *Science China Technological Sciences*, vol. 59, no. 10, pp. 1549–1558, 2016.

[20] X. X. Chen, P. He, and Z. Qin, "Damage to the microstructure and strength of altered granite under wet-dry cycles," *Symmetry-Basel*, vol. 10, pp. 1–13, 2018.

[21] L.-p. Cheng, C. Wang, L.-z. Tang et al., "Study on dynamic characteristics of deep siltstone under high static stress and frequent dynamic disturbance," *Advances in Civil Engineering*, vol. 2019, pp. 1–12, 2019.

[22] Y. Xu and F. Dai, "Dynamic response and failure mechanism of brittle rocks under combined compression-shear loading experiments," *Rock Mechanics and Rock Engineering*, vol. 51, no. 3, pp. 747–764, 2018.

[23] K. Liu, Q. B. Zhang, G. Wu, J. C. Li, and J. Zhao, "Dynamic mechanical and fracture behaviour of sandstone under multiaxial loads using a triaxial Hopkinson bar," *Rock Mechanics and Rock Engineering*, vol. 52, no. 7, pp. 2175–2195, 2019.

[24] H.-b. Du, F. Dai, Y. Xu, Y. Liu, and H.-n. Xu, "Numerical investigation on the dynamic strength and failure behavior of rocks under hydrostatic confinement in SHPB testing," *International Journal of Rock Mechanics and Mining Sciences*, vol. 108, pp. 43–57, 2018.

[25] H. B. Du, F. Dai, and Y. Xu, "Mechanical responses and failure mechanism of hydrostatically pressurized rocks under combined compression-shear impacting," *International Journal of Mechanical Sciences*, vol. 165, pp. 105–219, 2020.

[26] S.-Q. Yang, Y. Ju, F. Gao, and Y.-L. Gui, "Strength, deformability and X-ray micro-CT observations of deeply buried marble under different confining pressures," *Rock Mechanics and Rock Engineering*, vol. 49, no. 11, pp. 4227–4244, 2016.

[27] T. Meng, D. Zhang, Y. Hu, X. Jianlin, S. Sufang, and L. Xiaoming, "Study of the deformation characteristics and fracture criterion of the mixed mode fracture toughness of gypsum interlayers from Yunying salt cavern under a confining pressure," *Journal of Natural Gas Science and Engineering*, vol. 58, pp. 1–14, 2018.

[28] X. L. Xu and M. Karakus, "A coupled thermo-mechanical damage model for granite," *International Journal of Rock Mechanics and Mining Sciences*, vol. 103, pp. 195–204, 2018.

[29] X. Xu, F. Gao, and Z. Zhang, "Thermo-mechanical coupling damage constitutive model of rock based on the Hoek-Brown strength criterion," *International Journal of Damage Mechanics*, vol. 27, no. 8, pp. 1213–1230, 2018.

[30] X.-l. Xu, M. Karakus, F. Gao, and Z.-z. Zhang, "Thermal damage constitutive model for rock considering damage threshold and residual strength," *Journal of Central South University*, vol. 25, no. 10, pp. 2523–2536, 2018.

[31] L. Zhu, X. Xu, X. Cao, and S. Chen, "Statistical constitutive model of thermal damage for deep rock considering initial compaction stage and residual strength," *Mathematical Problems in Engineering*, vol. 2019, Article ID 9035396, 10 pages, 2019.

[32] S. J. Miao, H. Wang, M. F. Cai, Y. F. Song, and J. T. Ma, "Damage constitutive model and variables of cracked rock in a hydro-chemical environment," *Arabian Journal of Geosciences*, vol. 11, pp. 1–14, 2018.

[33] T. A. Bui, H. Wong, F. Deleruyelle, and A. Zhou, "Constitutive modelling of the time-dependent behaviour of partially saturated rocks," *Computers and Geotechnics*, vol. 78, pp. 123–133, 2016.

[34] P. Cao, Y. D. Wen, Y. X. Wang, H. P. Yuan, and B. X. Yuan, "Study on nonlinear damage creep constitutive model for high-stress soft rock," *Environmental Earth Science*, vol. 75, pp. 1–8, 2016.

[35] F. Wu, J. Chen, and Q. Zou, "A nonlinear creep damage model for salt rock," *International Journal of Damage Mechanics*, vol. 28, no. 5, pp. 758–771, 2019.

[36] Y.-L. Li and Z.-Y. Ma, "A damaged constitutive model for rock under dynamic and high stress state," *Shock and Vibration*, vol. 2017, Article ID 8329545, 6 pages, 2017.

[37] Z. L. Wang, H. Shi, and J. G. Wang, "Mechanical behavior and damage constitutive model of granite under coupling of temperature and dynamic loading," *Rock Mechanics and Rock Engineering*, vol. 51, no. 10, pp. 3045–3059, 2018.
[38] T. Yin, P. Wang, J. Yang, and X. Li, "Mechanical behaviors and damage constitutive model of thermally treated sandstone under impact loading," *IEEE Access*, vol. 6, pp. 72047–72062, 2018.
[39] Y. Liu and F. Dai, "A damage constitutive model for intermittent jointed rocks under cyclic uniaxial compression," *International Journal of Rock Mechanics and Mining Sciences*, vol. 103, pp. 289–301, 2018.
[40] X. S. Liu, J. G. Ning, Y. L. Tan, and Q. H. Gu, "Damage constitutive model based on energy dissipation for intact rock subjected to cyclic loading," *International Journal of Rock Mechanics and Mining Sciences*, vol. 85, pp. 27–32, 2016.
[41] F. Q. Gong, X. B. Li, and X. L. Liu, "Preliminary experimental study of characteristics of rock subjected to 3D coupled static and dynamic loads," *Chinese Journal of Rock Mechanics and Engineering*, vol. 30, pp. 1178–1190, 2011.
[42] C. A. Tang, *A Catastrophe in the Process of Rock Breaking*, China Coal Industry Publishing House, Beijing, China, 1993.
[43] Y. Zhu, *The Damage Theory of Mineral Rock Silt*, Northeast Institute of Technology, Jorhat, India, 1989.
[44] X. B. Li and D. S. Gu, *Rock Impact Dynamics*, Central South University of Technology Press, Changsha, China, 1994.
[45] Y. L. Zheng, C. Zhou, and S. Y. Xia, "Discussion on viscoelastic continuum damage constitutive model of rock and soil," *Journal of Hehai University*, vol. 25, pp. 114–116, 1997.
[46] G. Q. Zhou and X. M. Liu, *Viscoelascity Theory*, University of Science and Technology of China Press, Hefei, China, 1996.
[47] S. Kinoshita, K. Sato, and M. Kawakita, "On the mechanical behavior of rocks under impulsive loading," *Bulletin of the Faculty of Engineering Hokkaido University*, vol. 8, pp. 51–62, 1977.
[48] J. Yang, Q. K. Jin, and F. L. Huang, *Theoretical Model of Rock Blasting and Numerical Simulation*, Science Press, Beijing, China, 1999.
[49] J. Lemaitre and J. L. Chaboche, *Mechanics of Solid Materials*, Cambridge University Press, Cambridge, UK, 1990.